

Hybrid molecular beam epitaxy growth of BaTiO₃ films

Cite as: J. Vac. Sci. Technol. A **39**, 040404 (2021); <https://doi.org/10.1116/6.0001140>
Submitted: 11 May 2021 • Accepted: 02 June 2021 • Published Online: 24 June 2021

William Nunn, Sara Sandlass, Maike Wegner, et al.

COLLECTIONS

Paper published as part of the special topic on [Honoring Dr. Scott Chambers' 70th Birthday and His Leadership in the Science and Technology of Oxide Thin Films](#)

 This paper was selected as an Editor's Pick



View Online



Export Citation



CrossMark

ARTICLES YOU MAY BE INTERESTED IN

[Van der Waals epitaxy and remote epitaxy of LiNbO₃ thin films by pulsed laser deposition](#)


Journal of Vacuum Science & Technology A **39**, 040405 (2021); <https://doi.org/10.1116/6.0001109>

[Epitaxial integration of BaTiO₃ on Si for electro-optic applications](#)


Journal of Vacuum Science & Technology A **39**, 030804 (2021); <https://doi.org/10.1116/6.0000923>

[BaTiO₃-based piezoelectrics: Fundamentals, current status, and perspectives](#)

Applied Physics Reviews **4**, 041305 (2017); <https://doi.org/10.1063/1.4990046>



HIDEN
ANALYTICAL



40
YEARS
1982 - 2022


Instruments for Advanced Science

- Knowledge,
- Experience,
- Expertise

Click to view our product catalogue


Contact Hiden Analytical for further details:
www.HidenAnalytical.com
info@hideninc.com

Gas Analysis




- ▶ dynamic measurement of reaction gas streams
- ▶ catalysis and thermal analysis
- ▶ molecular beam studies
- ▶ dissolved species probes
- ▶ fermentation, environmental and ecological studies

Surface Science




- ▶ UHVTPD
- ▶ SIMS
- ▶ end point detection in ion beam etch
- ▶ elemental imaging - surface mapping

Plasma Diagnostics



- ▶ plasma source characterization
- ▶ etch and deposition process reaction kinetic studies
- ▶ analysis of neutral and radical species

Vacuum Analysis



- ▶ partial pressure measurement and control of process gases
- ▶ reactive sputter process control
- ▶ vacuum diagnostics
- ▶ vacuum coating process monitoring

Hybrid molecular beam epitaxy growth of BaTiO₃ films

Cite as: J. Vac. Sci. Technol. A **39**, 040404 (2021); doi: 10.1116/6.0001140

Submitted: 11 May 2021 · Accepted: 2 June 2021 ·

Published Online: 24 June 2021



View Online



Export Citation



CrossMark

William Nunn,¹ Sara Sandlass,¹ Maike Wegner,² Ryan Haislmaier,¹ Abinash Kumar,³ Malleswararao Tangi,¹ James LeBeau,³  Eckhard Quandt,² Richard D. James,⁴ and Bharat Jalan^{1,a)} 

AFFILIATIONS

¹Department of Chemical Engineering and Materials Science, University of Minnesota, Minneapolis, Minnesota 55455

²Institute for Materials Science, Kiel University, Kiel 24143, Germany

³Department of Materials Science and Engineering, Massachusetts Institute of Technology, Cambridge, Massachusetts 02139

⁴Department of Aerospace Engineering and Mechanics, University of Minnesota, Minneapolis, Minnesota 55455

Note: This paper is a part of the Special Collection Honoring Dr. Scott Chambers' 70th Birthday and His Leadership in the Science and Technology of Oxide Thin Films.

a) Author to whom correspondence should be addressed: bjalan@umn.edu

ABSTRACT

The ability to reproducibly synthesize thin films with precise composition and controlled structure is essential for fundamental study and mass production. Here, we demonstrate the hybrid molecular beam epitaxy (MBE) growth of epitaxial, single crystalline BaTiO₃ films with different thicknesses on Nb-doped SrTiO₃ substrates with atomically smooth surfaces. By combining scanning transmission electron microscopy, temperature-dependent high-resolution x-ray diffraction, reflection high-energy electron diffraction, and atomic force microscopy, we study the effect of growth conditions and the interplay between stoichiometry and epitaxial strain on the resulting structure. Furthermore, we demonstrate a close to bulk-like ferroelectric phase transition in thicker films and highlight the effect of strain on the phase transition temperature. This work establishes the hybrid MBE approach for the growth of heteroepitaxial BaTiO₃ films on conducting substrates with scalable thickness and controlled stoichiometry.

Published under an exclusive license by the AVS. <https://doi.org/10.1116/6.0001140>

I. INTRODUCTION

BaTiO₃ (BTO) is a prototypical ferroelectric perovskite oxide that has been extensively studied for applications such as dielectrics,¹ ferroelectric random-access memory,^{2,3} lead-free capacitors,⁴ photonic devices,⁵ and ferroelectric energy conversion devices.^{6,7} BTO has room-temperature ferroelectricity with a Curie temperature, T_c , of ~ 120 °C.⁸ With a tetragonal unit cell at room temperature, bulk BTO has lattice parameters of 3.992 and 4.036 Å along what is commonly denoted as the a axis and c axis, respectively.⁹ At T_c , BTO undergoes a first-order phase transition to a paraelectric cubic structure accompanied by a large change in the dielectric constant. These characteristics, which have led to it being one of the most studied ferroelectrics, are significantly dependent on its structure, which in turn can be heavily influenced by the cation and oxygen stoichiometry. Controlling the stoichiometry in BTO

has been challenging in thin film form and the source of many investigations on these materials.^{10,11}

Growth of thin film BTO has been reported using various thin film deposition techniques including molecular beam epitaxy (MBE), an ultrahigh vacuum, low-energy deposition process. MBE has the advantages of being able to produce materials with atomic-layer control and low in impurities, leading to high quality BTO films.^{12–14} MBE growth of BTO films can prove difficult; however, mostly due to the problem associated with stoichiometry control. Regulating the relative Ba/Ti metal fluxes is often challenging, and, in oxide MBE, oxygen deficiency can also occur as a relatively low oxygen background pressure ($\sim 10^{-5}$ – 10^{-6} Torr) must be used to maintain the characteristic MBE large mean-free path. While oxygen deficiency can be overcome by postgrowth annealing, controlling cation stoichiometry is still a major challenge.

Recently, advances have been made in MBE synthesis to include metal-organic-based hybrid MBE techniques that replace solid elemental metal sources with metal-organic compounds. Using this approach, it has been shown that an adsorption-controlled “MBE growth window” for self-regulating stoichiometry exists for a variety of compounds, including titanates,^{12,15,16} vanadates,¹⁷ and stannates.¹⁸ Of the titanates, a few reports exist for BTO involving hybrid MBE growth; however,^{12,19–22} only one report directly addresses the growth window.¹² BTO was shown to grow completely coherently on an insulating GdScO₃ substrate where the growth window was identified by a Ba to Ti flux ratio region within which films displayed a constant out-of-plane lattice parameter.¹² Here, we take a closer look at the growth of BTO films using hybrid MBE and study the effect of growth conditions and film thickness when grown on the more commonly used conducting Nb-doped SrTiO₃ (Nb:STO) substrates, which can be used as a bottom metal electrode for ferroelectric capacitor structure.

II. EXPERIMENT

Hybrid MBE growth of BaTiO₃ films was performed using solid elemental Ba sublimated in an effusion cell and the metal-organic precursor titanium (IV) tetraisopropoxide supplied through an external gas inlet system. Films were grown in the presence of oxygen supplied at a pressure of $\sim 5 \times 10^{-6}$ Torr by a radio frequency plasma source operated at 250 W. Films were grown on Nb:STO (001) substrates following a 20 min *in situ* surface cleaning by exposure to oxygen plasma at growth temperature. Films were grown at a substrate temperature of 950 °C as determined by a thermocouple. Relative growth conditions were determined from the ratio of the Ti:Ba fluxes measured as a beam equivalent pressure (BEP) using a beam flux monitor inserted below the substrate prior to growth. Growth rates ranged from ~ 50 to 60 nm/h. Following completion of growth, the films were cooled down in oxygen.

Postgrowth annealing was done in an oxygen-rich environment after initial characterizations in a tube furnace operated at 900 °C for 1 h.

Reflection high-energy electron diffraction (RHEED) was carried out *in situ* during and after growth to monitor the film surfaces. Film surfaces after growth were also characterized using atomic force microscopy (AFM). High-resolution x-ray diffraction (HRXRD) and reciprocal space maps (RSM) were performed using a Rigaku SmartLab XE system.

Cross-sectional scanning transmission electron microscopy (STEM) samples of the BTO thin film were prepared using mechanical wedge polishing followed by Ar ion milling to obtain an electron transparent sample. STEM imaging was performed using a probe-corrected FEI Titan G2 60–300 kV S/TEM equipped with an extreme field emission gun and was operated at 200 kV with a beam current of 50 pA and probe convergence semiangle of 19.6 mrad. The high-angle annular dark field STEM (HAADF-STEM) collection inner semiangle was 77 mrad. Drift and scan distortion correction were applied using the revolving STEM approach.²³

III. RESULTS AND DISCUSSION

A representative HRXRD pattern for a BTO film grown on Nb:STO is shown in Fig. 1(a). Single peaks are present for the (001) planes showing single crystalline, epitaxial films consistent with the single domain structure of the tetragonal *c* axis oriented out-of-plane. Finite thickness fringes, evidence of high structural quality on a short lateral length scale, were present around the (001) peak. The surface of the BTO film consisted of atomic step terraces as seen in AFM and sharp streaky RHEED images with a 2× reconstruction along the [100] substrate azimuth [Figs. 1(b) and 1(c)], both attesting to the smooth surface morphology of the film.

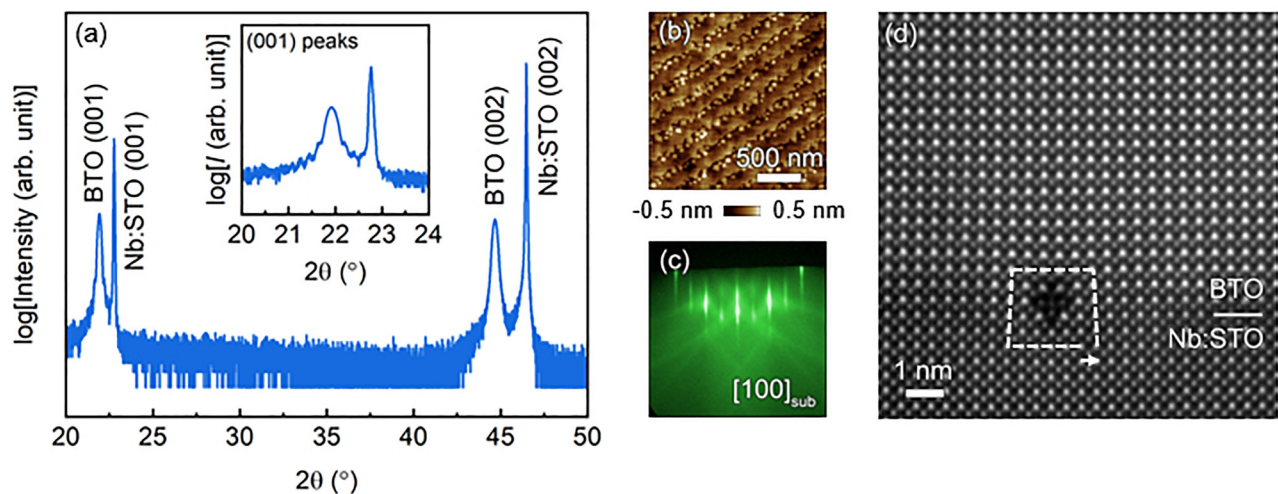


FIG. 1. (a) HRXRD, (b) AFM, and (c) RHEED of 46 nm BTO/Nb-doped STO (001) Ti:Ba BEP ratio of 13.7. The inset of (a) shows a zoomed-in look at the (001) peak. (d) Cross-sectional HAADF-STEM image of the film-substrate interface of thicker 240 nm BTO grown on Nb-doped STO (001), viewed along the [100] zone axis. The dashed white line draws the Burgers circuit around a misfit dislocation with the white arrow signifying the Burgers vector $\mathbf{b} = a[010]$.

To take a closer look at these films, cross-sectional HAADF-STEM was performed on a thicker 240 nm BTO film grown on Nb:STO [Fig. 1(d)]. An atomically abrupt film-substrate interface was found, however, with misfit dislocations sporadically distributed along the interface. This observation of misfit dislocations is consistent with relaxing films owing to a large lattice mismatch of -2.2% for the BTO film grown on STO. However, the thinner films, e.g., 42 nm shown in Figs. 1(a)–1(c), showed an expanded out-of-plane lattice parameter (a_{op}) obtained from HRXRD, $4.058 \pm 0.002 \text{ \AA}$ compared to the bulk value of 4.036 \AA ,

suggesting these thinner films are still strained. While the presence of strain is likely responsible for the expanded a_{op} , it can also be argued to be due to nonstoichiometric related defects. To further investigate the effect of nonstoichiometry and strain relaxation as well as the interplay between the two, we grew two series of samples: (1) with varying Ti:Ba BEP flux ratios and (2) with varying thicknesses at a fixed Ti:Ba BEP ratio.

We first discuss the effect of Ti:Ba BEP ratio on films' structure and surface morphology. Figure 2(a) plots a_{op} versus Ti:Ba BEP ratio before and after a 1 h anneal in an oxygen-rich

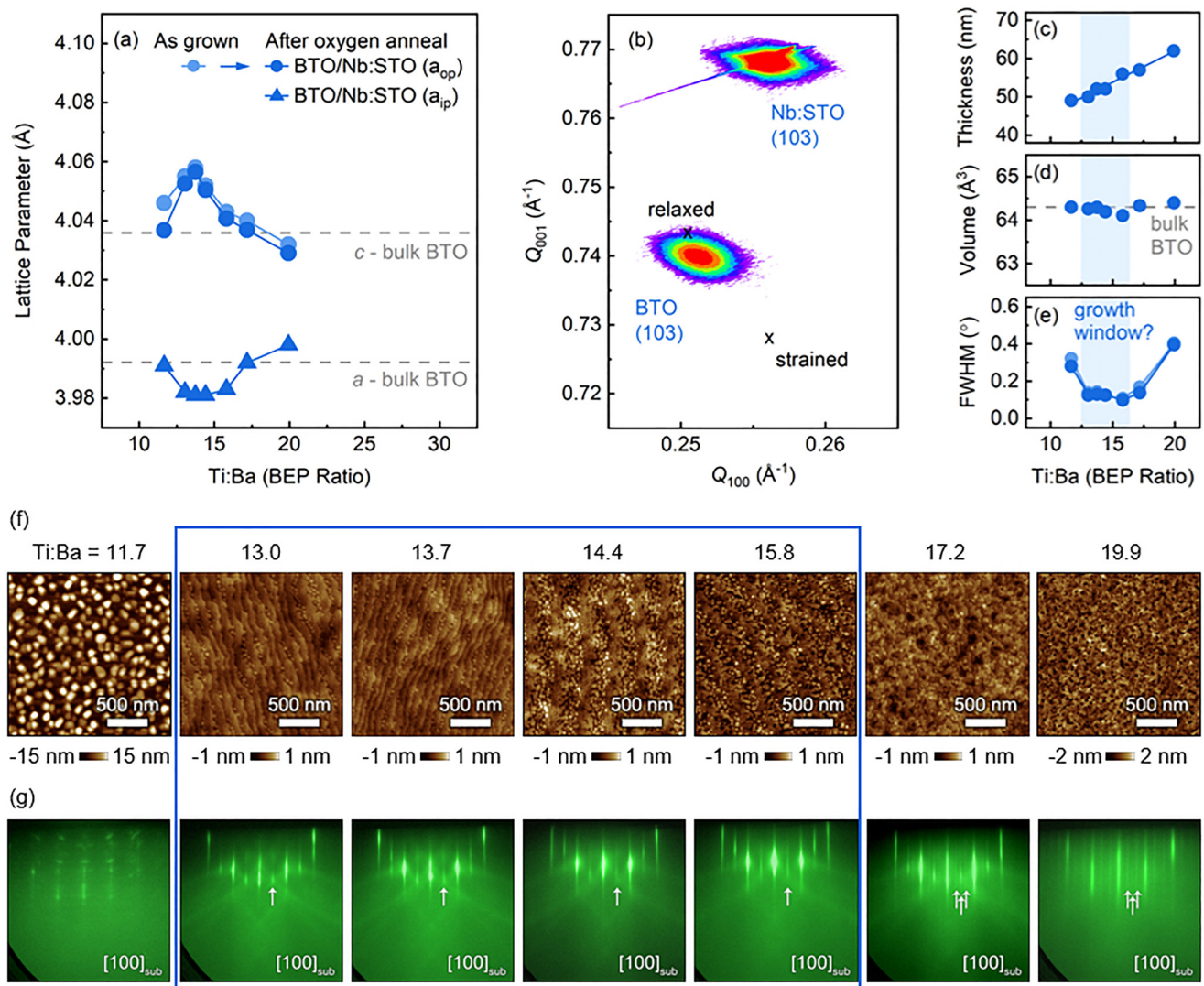


FIG. 2. (a) Lattice parameters of BTO films grown on Nb:STO before (light color) and after (dark color) oxygen annealing. (b) (103) RSM of BTO film at the peak lattice parameter growth condition Ti:Ba = 13.7. (c) Thickness, (d) unit cell volume, (e) FWHM of the (002) rocking curve, (f) AFM and (g) RHEED images along the substrate [100] azimuth with varying Ti:Ba growth conditions. White arrows mark surface reconstruction streaks.

environment at 900 °C. The purpose of the anneal was to decrease oxygen vacancies, which are commonly found in MBE-grown BTO films.²⁴ All films showed a decrease in a_{op} after annealing, which is most likely due to the filling of oxygen vacancies and/or further strain relaxation. At a first glance, from the trend in a_{op} versus Ti:Ba BEP ratio, the MBE growth window, as reported previously for the hybrid MBE of BTO films,¹² is not evident. The increase and then a decrease in a_{op} with increasing Ti:Ba contradicts the previous hybrid MBE report of a constant a_{op} with Ti:Ba for a fully coherent film on GdScO₃. However, the case of BTO grown on STO is more complicated due to the expected strain relaxation from the significant lattice mismatch (−2.2%) as opposed to when grown on GdScO₃, which has approximately a −0.5% lattice mismatch.

To this end, we measured the RSM of the films to determine the strain state. Figure 2(b) shows the RSM of a 53 nm film that had the largest a_{op} , grown at Ti:Ba = 13.7, which revealed a mostly, but not completely, relaxed film as evidenced by the film peak being between the expected relaxed and strained positions. It should be noted that the coherently strained in-plane lattice parameter (a_{ip}) of a BTO film on STO substrates refers to the lattice parameter of cubic STO, 3.905 Å, whereas the expected coherently strained a_{op} , 4.121 Å, was calculated using the BTO elastic constants C_{11} and C_{33} as shown in Eq. (1), where ϵ_{ip} is the in-plane strain applied to BTO from the substrate,²⁵

$$a_{op}(\text{coherent}) = a_{op}(\text{bulk}) \left[1 - \frac{2 \times C_{11} \times \epsilon_{ip}}{C_{33}} \right]. \quad (1)$$

The expanded a_{op} of the BTO film grown here can, therefore, be explained by the residual strain present in the film and the partial relaxation. This observation is further consistent with presence of the misfit dislocations in our STEM image in Fig. 1(d).

Nevertheless, the increasing and then decreasing trend in a_{op} seen in Fig. 2(a) does raise questions on the stoichiometry of these films. If an MBE growth window does exist, we expect to see a range of flux ratios within which there is adsorption-controlled stoichiometric growth signified by a constant a_{op} for a coherent film. For our BTO growth, we do not see this due to strain relaxation. However, we do expect an adsorption-controlled growth regime to occur when using this hybrid MBE technique as demonstrated earlier.¹² We did find, when taking into account not only a_{op} but also a_{ip} obtained from RSMs (Fig. S1),²⁸ a nearly constant volume, assuming a tetragonal unit cell, of $64.3 \pm 0.1 \text{ \AA}^3$, the value of bulk BTO. This can be seen in Fig. 2(d) throughout the Ti:Ba ratios used here. Along with a constant and low full width at half maximum (FWHM) of the (002) BTO film rocking curves in the center of these growth series [Fig. 2(e)], it is possible that an adsorption-controlled window is present but the more complex strain state of BTO/Nb:STO causes the changes seen in a_{op} . At the very least, any nonstoichiometric related defects present within this flux range do not have an effect on the structural quality that can be probed by XRD.

Consistent with the above observation, films grown within this flux range also showed atomically smooth surface morphology with step edges [Fig. 2(f)] along with identical 2× surface reconstruction

[Fig. 2(g)]. Moving to a Ba-rich regime (low Ti:Ba), an island growth mode was seen with spotty RHEED and large island formations in AFM. On the other side, the Ti-rich regime (Ti:Ba ≥ 17.2), a transition away from steps on the surface was seen with the emergence of 3× reconstruction in RHEED. The nonstoichiometry present in the film not only increases bulk structural disorder, as seen by the FWHM, but also the growth mode and surface morphology. The drastic change in surface morphology as moving to the Ba-rich regime is in contrast with the hybrid MBE growth of SrTiO₃. In the case of SrTiO₃, moving off stoichiometry toward both the Sr- and Ti-rich regime does not cause such levels of surface roughening, suggesting the difference in growth behavior for Ba versus Sr in oxide hybrid MBE.

To further check the film's cation stoichiometry and probe the strain relaxation, we performed a thickness-dependent study on a representative BTO growth condition. Figure 3(a) shows the HRXRD patterns of films, ranging in thickness from 20 to 500 nm, grown at the peak a_{op} growth condition in Fig. 2(a), Ti:Ba BEP = 13.7. As expected, due to strain relaxation, we saw a peak shift to larger 2θ with increasing thickness. The a_{op} obtained from these peak positions, shows this expected decrease, settling to approximately the bulk lattice parameter at a thickness of 115 nm, as seen in Fig. 3(b). The lack of strain was confirmed by RSM (Fig. S2)²⁸ of the thickest sample, 500 nm BTO on Nb:STO where

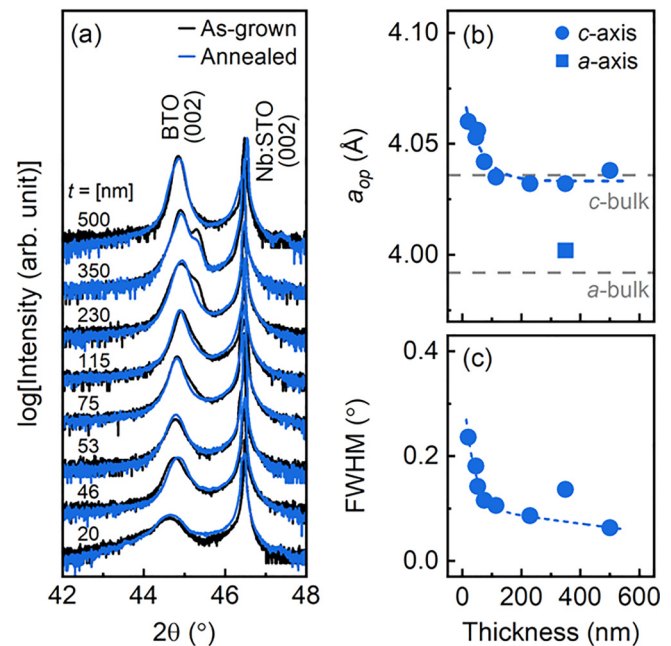


FIG. 3. (a) HRXRD of 20–500 nm BTO samples before and after oxygen annealing, increasing in thickness from bottom to top. (b) Thickness-dependent out-of-plane lattice parameter taken from both peaks when present, representing c and a axis domains. (c) FWHM of (002) film rocking curves. All films were grown at the peak lattice parameter growth condition, Ti:Ba = 13.7. Values reported in panels (b) and (c) are taken after oxygen annealing.

the film peak aligned with the expected bulk relaxed position. Films also showed a decrease in the (002) film rocking curve FWHM with increasing thickness [Fig. 3(c)] suggesting improved crystallinity. Interestingly, after strain relaxation was complete as films were grown to larger thicknesses, we found the emergence of both *c*- and *a*-domains. A second peak began to appear in the HRXRD, for all but the thickest 500 nm film, signifying a second domain consistent with the *a* axis of BTO aligned out-of-plane. This agrees well with what has been shown for BTO films that the absence of biaxial in-plane compressive strain helps form multidomain films, not only the *c* axis orientation.²⁶ Remarkably, however, postoxygen annealing was found to decrease or even eliminate *a*-domains (depending on the film thicknesses) as evident from the lowering of the peak intensity associated with the *a*-domains [Fig. 3(a)].

With the growth condition effect on the stoichiometry and strain state determined, we studied the effect of temperature on the lattice parameters of these films. Figure 4 shows the a_{op} obtained from temperature-dependent HRXRD of 50 and 350 nm BTO films. Consistent with the first-order phase transition in a bulk BTO single crystal, the 350 nm BTO film showed a close to bulk phase transition temperature,⁹ with only a slight increase in T_c . On the other hand, the thinner 50 nm film yielded a phase transition with significantly higher T_c (also see Fig. S3),²⁸ following the known trend of an increased T_c with increased strain.²⁷

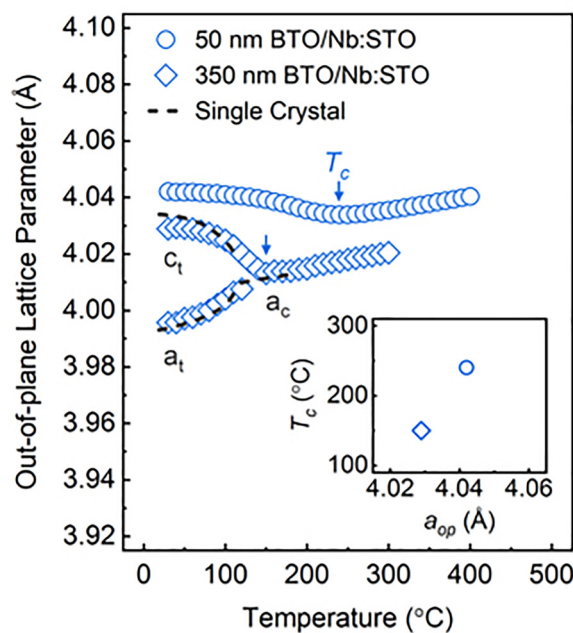


FIG. 4. Temperature-dependent out-of-plane lattice parameters of 50 and 350 nm BTO films grown on Nb:STO with Ti:Ba = 13.7. Arrows mark Curie temperatures (T_c). Dashed gray line is bulk single crystal *c*-domain (c_t) and *a*-domain tetragonal (a_t) as well as cubic (a_c) lattice parameters. Inset shows the Curie temperature changing with the out-of-plane lattice parameter.

In summary, single crystalline, epitaxial BTO films were grown on a conducting Nb-doped STO films using hybrid MBE. Samples grown within the “MBE growth window” yielded films with a constant lattice volume, low FWHM, and atomically smooth surface morphologies with an identical $2\times$ reconstruction in RHEED. With increasing film thickness, BTO films begin to relax, reaching to bulk lattice parameters at film thicknesses ≥ 115 nm. A close to bulk phase transition temperature was demonstrated in a 350 nm BTO film on an Nb:STO substrate with a slightly increased T_c of $\sim 150^\circ\text{C}$. Consistent with prior results, in-plane strain was found to raise T_c . This work shows the influence of stoichiometry and strain relaxation the BTO film structure and surface morphology in addition to establishing the hybrid MBE for a stoichiometric, epitaxial BTO film on a conducting Nb-doped STO substrate, which is much needed to create all-epitaxial perovskite capacitor structures.

AUTHORS' CONTRIBUTIONS

W.N. grew samples with help from R.H. and M.T. W.N., S.S., R.H. and M.T. performed HRXRD and AFM characterization. W.N. and M.W. performed temperature-dependent HRXRD. A.K. performed TEM sample preparation and STEM imaging under the guidance of J.L. W.N. and B.J. wrote the manuscript. All authors contributed to the discussion and manuscript preparation.

ACKNOWLEDGMENTS

This work was primarily supported by the U.S. Department of Energy under Grant No. DE-SC002021. The work also benefited from the Norwegian Centennial Chair Program (NOCC) and Vannevar Bush Faculty Fellowship. M.W. and E.Q. acknowledge funding from the Deutsche Forschungsgemeinschaft (DFG) through a Reinhart Koselleck Project (No. 313454214). J.L. and A.K. acknowledge support for this work from the National Science Foundation (No. DMR-1350273). A.K. acknowledges support from an MIT Mathworks Engineering Fellowship. Parts of this work were carried out at the Characterization Facility, University of Minnesota, which receives partial support from the NSF through the MRSEC program under Award No. DMR-2011401, as well as the Analytical Instrumentation Facility (AIF) at North Carolina State University, which is supported by the State of North Carolina and the National Science Foundation (No. ECCS-1542015). AIF is a member of the North Carolina Research Triangle Nanotechnology Network (RTNN), a site in the National Nanotechnology Coordinated Infrastructure (NNCI).

The authors declare no competing interests.

DATA AVAILABILITY

The data that support the findings of this study are available within the article and its supplementary material.²⁸ Additional data that support the findings of this study are available from the corresponding author upon reasonable request.

REFERENCES

1. A. I. Kingon, J.-P. Maria, and S. K. Streiffer, *Nature* **406**, 1032 (2000).
2. N. Setter *et al.*, *J. Appl. Phys.* **100**, 051606 (2006).

- ³R. Ramesh, S. Aggarwal, and O. Auciello, *Mater. Sci. Eng. R Rep.* **32**, 191 (2001).
- ⁴H. Zhang *et al.*, *J. Mater. Chem. C* **8**, 16648 (2020).
- ⁵S. Abel *et al.*, *Nat. Commun.* **4**, 1671 (2013).
- ⁶A. Bucsek, W. Nunn, B. Jalan, and R. D. James, *Phys. Rev. Appl.* **12**, 034043 (2019).
- ⁷A. N. Bucsek, W. Nunn, B. Jalan, and R. D. James, *Annu. Rev. Mater. Res.* **50**, 283 (2020).
- ⁸K. Sakayori *et al.*, *Jpn. J. Appl. Phys.* **34**, 5443 (1995).
- ⁹H. F. Kay, *Acta Crystallogr.* **1**, 229 (1948).
- ¹⁰J. L. MacManus-Driscoll, M. P. Wells, C. Yun, J.-W. Lee, C.-B. Eom, and D. G. Schlom, *APL Mater.* **8**, 040904 (2020).
- ¹¹D. G. Schlom, *APL Mater.* **3**, 062403 (2015).
- ¹²Y. Matsubara, K. S. Takahashi, Y. Tokura, and M. Kawasaki, *Appl. Phys. Express* **7**, 125502 (2014).
- ¹³L. Mazet, S. M. Yang, S. V. Kalinin, S. Schamm-Chardon, and C. Dubourdieu, *Sci. Technol. Adv. Mater.* **16**, 036005 (2015).
- ¹⁴Y. Yoneda, T. Okabe, K. Sakaue, H. Terauchi, H. Kasatani, and K. Deguchi, *J. Appl. Phys.* **83**, 2458 (1998).
- ¹⁵B. Jalan, R. Engel-Herbert, N. J. Wright, and S. Stemmer, *J. Vac. Sci. Technol. A* **27**, 461 (2009).
- ¹⁶B. Jalan, P. Moetakaf, and S. Stemmer, *Appl. Phys. Lett.* **95**, 032906 (2009).
- ¹⁷J. A. Moyer, C. Eaton, and R. Engel-Herbert, *Adv. Mater.* **25**, 3578 (2013).
- ¹⁸A. Prakash, J. Dewey, H. Yun, J. S. Jeong, K. A. Mkhoyan, and B. Jalan, *J. Vac. Sci. Technol. A* **33**, 060608 (2015).
- ¹⁹J. Cheng *et al.*, *IEEE Electron Device Lett.* **41**, 621 (2020).
- ²⁰J. M. LeBeau, A. J. D'Alfonso, N. J. Wright, L. J. Allen, and S. Stemmer, *Appl. Phys. Lett.* **98**, 052904 (2011).
- ²¹S. Raghavan, J. Y. Zhang, O. F. Shoron, and S. Stemmer, *Phys. Rev. Lett.* **117**, 037602 (2016).
- ²²O. F. Shoron, S. Raghavan, C. R. Freeze, and S. Stemmer, *Appl. Phys. Lett.* **110**, 232902 (2017).
- ²³X. Sang and J. M. LeBeau, *Ultramicroscopy* **138**, 28 (2014).
- ²⁴G. Niu, B. Gautier, S. Yin, G. Saint-Girons, P. Lecoeur, V. Pillard, G. Hollinger, and B. Vilquin, *Thin Solid Films* **520**, 4595 (2012).
- ²⁵R. Bechmann, *J. Acoust. Soc. Am.* **28**, 347 (1956).
- ²⁶V. Vaithyanathan *et al.*, *J. Appl. Phys.* **100**, 024108 (2006).
- ²⁷K. J. Choi *et al.*, *Science* **306**, 1005 (2004).
- ²⁸See supplementary material at <https://doi.org/10.1116/6.0001140> for the reciprocal space maps of BTO films as a function of growth conditions and thickness as well for the temperature-dependent x-ray diffraction patterns revealing the close to bulk-like phase transition.